Scalloping Suppression Method for ScanSAR Images Considering Azimuthal Correction Errors and Range Spatial Variant Characteristics

Hao Ye, Guowang Jin, Hongmin Zhang, Xin Xiong, Jiajun Wang, and He Yang

***Abstract*—Scanning synthetic aperture radar (ScanSAR) is the dominant imaging mode of existing SAR satellites. However, in this mode, a burst operation is utilized, resulting in scalloping problems that significantly impact the quality of ScanSAR images. In response to the poor robustness and high complexity of existing denoising algorithms, and based on the analysis of the causes of scalloping, a scalloping suppression method for ScanSAR images that considers azimuthal correction errors and range spatial variant characteristics is proposed. First, estimating the azimuth antenna pattern (AAP) correction error by analyzing the alternating scalloping periods and intensities along the azimuth. Next, a cubic polynomial is used to fit the variation in the noise gain along the range. Then, scalloping is removed from both the azimuth and range. Finally, the performance of the method is validated via Gaofen-3 ScanSAR images of different scenes. The results demonstrate that the proposed method can effectively remove scalloping, adapt well to complex scenes, and retain image details.**

***Index Terms*—Scalloping suppression, scanning synthetic aperture radar (ScanSAR), azimuthal correction error, range spatial variant characteristic, Gaofen-3.**

I. Introduction

Synthetic aperture radar (SAR) is characterized by its all-weather, all-day operation, wide coverage, and excellent penetration capabilities, which contribute to its extensive use in fields such as environmental monitoring and target identification [1], [2]. Existing SAR satellites have various imaging modes, but scanning SAR (ScanSAR) is the dominant imaging mode [3]. In the ScanSAR imaging mode, a wide mapping swath can be achieved, and the repetitive observation cycle needed for global coverage may be significantly shortened. However, the scanning mechanism used during the ScanSAR imaging process leads to a time-varying system transfer function. In addition, there are periodic variations in the total gain of the system in the azimuth, leading to periodic fluctuations in the output signal intensity along the azimuth. This phenomenon is commonly referred to as the scalloping problem [4], [5].

The presence of scalloping significantly reduces the quality of images, increases the difficulty of image interpretation, and affects subsequent imaging applications. Therefore, many scholars have researched descalloping methods for ScanSAR images. Theoretically, scalloping can be eliminated during imaging by accurately compensating for the azimuth antenna pattern (AAP). Scalloping is removed by many scholars during the imaging process through the estimation of AAP [6]–[9]. However, owing to AAP estimation errors, significant scalloping remains evident in ScanSAR images [9]. Accordingly, several methods for removing scalloping in image postprocessing have been proposed recently. These postprocessing methods can be categorized into two main groups: frequency domain (including wavelet domain [10]) processing and spatial domain processing. The most straightforward descalloping method involves identifying peaks in the average power spectrum and applying median filtering to mask these peaks [3], [11]. Nonetheless, the inability to ensure that the removed frequency bands do not contain useful scene information such as edges or slopes is an inherent problem in frequency-domain denoising methods. Therefore, the frequency-domain descalloping method is utilized primarily for ScanSAR images without obvious features such as calm seas and is unsuitable for complex scenes.

Spatial domain scalloping suppression is the most widely applied descalloping method. Since Iqbal [12] introduced the Kalman filter to eliminate scalloping, several enhancements to the filter aimed at addressing its theoretical limitations have been reported [13], [14]. And Tian [15] performed scalloping suppression in the spatial domain via weighted filtering. Most spatial domain filtering methods assume that the scalloping intensity remains constant in the range direction. Indeed, scalloping can also vary in range because of the effects of AAP compensation during the imaging process and platform instability. This assumption is applicable in a small area,

Manuscript received ,; revised , .

This work was supported in part by the National Natural Science Foundation of China under Grant 42201492, in part by the National Key R&D Program of China under Grant 2023YFB2604001, and in part by 2022 Transportation Research Funding Plan of Henan under Grant 2022-3-2. *(Corresponding author:Guowang Jin.)*

H. Ye is with the Institute of Geospatial Information, PLA Strategic Support Force Information Engineering University, Zhengzhou 450001, China. (e-mail: yehao_xd@163.com)

G. Jin and X. Xiong are with the Institute of Geospatial Information, PLA Strategic Support Information Engineering University, Zhengzhou 450001, China, and also with the Key Laboratory of Smart Earth, Beijing 100094, China. (e-mail: guowang_jin@163.com; xiongxinhbhh@163.com)

H. Zhang is with the Institute of Data and Target Engineering, PLA Strategic Support Force Information Engineering University, Zhengzhou 450001, China. (e-mail: zhmin1206@163.com)

J. Wang is with the Institute of Geospatial Information, PLA Strategic Support Information Engineering University, Zhengzhou 450001, China, and also with the 92556 Troops, Ningbo 315000, China. (wangjiajunrs@126.com)

H. Yang is with the Transportation Development Center of Henan Province, Zhengzhou 450001, China. (e-mail:yanghe8813@163.com)

but in regions with wide ranges, it is necessary to perform block processing [14]. Moreover, most existing spatial domain methods need to divide images into stable and nonstable regions via different processing strategies for descalloping. This repeated division of images increases the complexity of the method, and the effectiveness of scalloping removal at region boundaries can also be compromised.

A scalloping suppression method for ScanSAR images is proposed in this letter, focusing on addressing the drawbacks of existing descalloping methods, such as poor robustness and high complexity, by considering azimuthal correction error and range spatial variant characteristics. First, by analyzing the scalloping model, the influence of scalloping is decomposed into AAP correction errors and range noise gain. Then, scalloping can be effectively removed in two dimensions through azimuthal correction error estimation and range noise gain polynomial fitting. Finally, the proposed method is tested on Chinese Gaofen-3 (GF-3) ScanSAR images. The results show that the proposed method can adapt well to complex scenes, leading to effective scalloping suppression.

This letter is organized as follows. Section II briefly introduces the ScanSAR model, followed by an analysis of the causes and characteristics of scalloping. In Section III, the proposed method is described in detail. Experimental validation of the proposed method is presented in Section IV, and conclusions are drawn in Section V.

II. Scalloping Modeling and Characterization

A. Scalloping modeling

To eliminate scalloping during the imaging process, a correction function is utilized to correct the AAP [3], [9]. However, when the correction function is applied, the presence of Doppler center estimation errors causes radiometric errors, reducing the correction accuracy and thus leading to residual scalloping. In this letter, residual scalloping and initial scalloping are collectively referred to as scalloping without differentiation. Additionally, due to the influence of platform instability during the imaging process, scalloping varies along the range [11]. Assuming that the Doppler center error shifts the AAP $G_a(x)$ by Δx, for ScanSAR images after image processing, the effect of scalloping can be represented as:

$$\begin{aligned} S_c(r,x) &= \frac{G_a(x)\cdot G_r(r,x)\cdot S_0(r,x)}{G_a(x+\Delta x)} \\ &= G_x(x)\cdot G_r(r,x)\cdot S_0(r,x) \end{aligned} \tag{1}$$

where r is the range coordinate, x is the azimuthal coordinate, $G_a(x)$ is the AAP expressed in the azimuthal coordinate, $G_r(r,x)$ is the range gain of the scalloping noise, $G_x(x)$ is the compensation error of the correction function for the scalloping along the azimuthal direction, $S_0(r,x)$ denotes the ScanSAR image without scalloping noise, and $S_c(r,x)$ denotes that the ScanSAR image contains scalloping noise.

B. Characteristics of scalloping in ScanSAR images

Fig. 1 shows an image of Hainan Island captured by GF-3 in the ScanSAR mode (Strip 1) on July 17, 2020. Significant

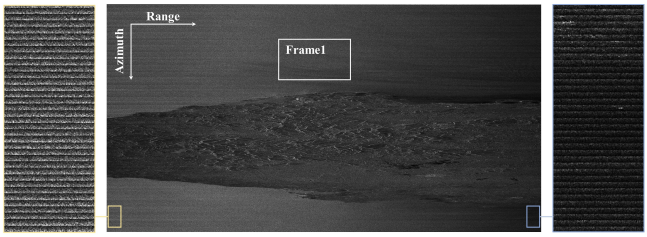

Fig. 1. GF-3 ScanSAR image (Strip 1).

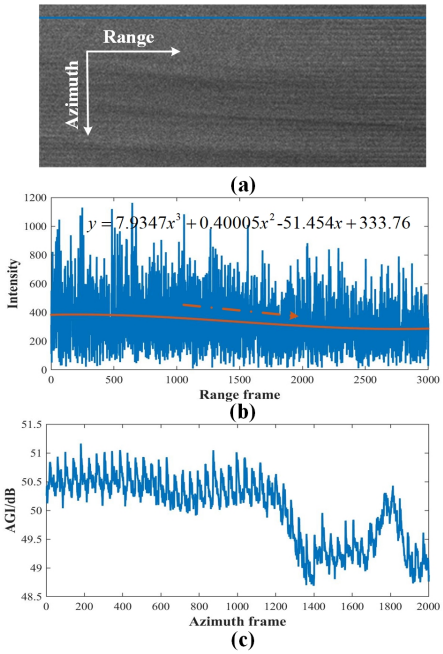

Fig. 2. Scalloping in frame 1: (a) original image, (b) intensity statistics along the range toward the blue line, (c) AGI of the image along the azimuth.

brightness variations from left to right can be observed in Fig. 1. These variations are caused by the lack of range spreading loss correction.

The following results of the intensity statistics of frame 1 along the range and azimuth are presented to observe the distribution characteristics of scalloping in the image. The intensity distribution of scalloping along the azimuth direction can be represented as:

$$g_c(x) = \frac{\sum_{r=1}^{m} p(r,x)}{m}, \quad y = 1,\ldots,n \tag{2}$$

where $p(r,x)$ is the image pixel intensity, m and n are the numbers of range and azimuth sampling points of the image. The average gray intensity (AGI) of scalloping along the azimuth direction can be expressed as [13]:

$$AGI(x) = 20\cdot\log_{10}\left[g_c(x)\right], \quad y = 1,\ldots,n \tag{3}$$

The statistical results of frame 1 scalloping are shown in Fig. 2. The formula in Fig. 2(b) represents the polynomial fitting result, with the red solid line depicting the function graph of the polynomial, and the red dashed line illustrating the decreasing trend exhibited by the polynomial function. By fitting a cubic polynomial to the intensity values in Fig. 2(b), it

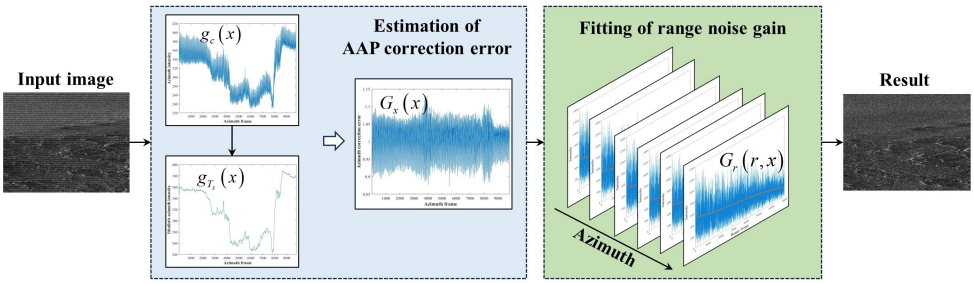

Fig. 3. Flowchart of the proposed descalloping scheme.

is clear that the intensity values change slowly along the range with a decreasing trend. We refer to the variation in scalloping along the range direction as the range noise gain and consider it to be the gain of the azimuthal variation in scalloping in the range direction. In Fig. 2(c), an evident sawtooth variation along the azimuth can be observed in the AGI, indicating that the scalloping noise is periodic.

III. Method

From the ScanSAR images and the scalloping model, the following characteristics of scalloping noise are noted: (1) scalloping occurs along the azimuth and extends across the entire swath in the range periodically, with the most pronounced scalloping generated at two adjacent burst transitions; (2) there is periodicity in the azimuth, manifested as bright and dark bands that alternate; and (3) owing to the instability of the platform, the introduced noise gain causes variations in scalloping along the range rather than remaining constant.

Fig. 3 shows the flowchart of the proposed descalloping scheme. The main steps involve estimating the AAP correction error and fitting the range noise gain. On the basis of the estimation results of the AAP correction error and range noise gain, scalloping suppression can be achieved by inverting Eq. 1, namely:

$$S_0(r,x) = S_c(r,x) / \left[G_x(x) \cdot G_r(r,x)\right] \tag{4}$$

A. Estimation of the AAP correction error

To obtain the AAP correction error, the periodicity of scalloping alternating along the azimuth needs to be estimated. The intensity distribution of scalloping along the azimuth is calculated via Eq. 2, and a series of local maxima in this distribution are identified:

$$\text{locs} = \text{findpeaks}\left[g_c(x)\right] \tag{5}$$

where locs denotes the location of the n local maxima values. By calculating the differences in locations between adjacent local maxima values, the periodicity of scalloping that alternates in strength along the azimuth direction ($n-1$ periods total) is determined. Additionally, to minimize the estimation error, the multiple period values obtained from the estimation are averaged to derive the final estimated period T_s. Then, a filtering window of appropriate size is created, and the mean of $g_c(x)$ is calculated across adjacent periods to obtain an azimuth intensity distribution without the influence of scalloping [15]:

$$g_{T_s}(x) = \begin{cases} \dfrac{\sum_{i=1}^{T_s} g_c(i)}{T_s}, & 1 \le x < \frac{T_s}{2}+1 \\ \dfrac{\sum_{i=x-T_s/2}^{x+T_s/2-1} g_c(i)}{T_s}, & \frac{T_s}{2}+1 \le x \le c-\frac{T_s}{2}+1 \\ \dfrac{\sum_{i=n-T_s+1}^{n} g_c(i)}{T_s}, & c-\frac{T_s}{2}+1 < x \le c \end{cases} \tag{6}$$

where $g_{T_s}(x)$ denotes the azimuth intensity distribution that is free from scalloping. By combining $g_{T_s}(x)$ and $g_c(x)$, the azimuthal compensation error can be calculated via the following equation:

$$G_x(x) = g_{T_s}(x)/g_c(x), \quad x = 1,\ldots,n \tag{7}$$

B. Fitting of the range noise gain

In Fig. 2, the scalloping variation in the range is observed. This variation does not exhibit distinct and periodic patterns as the azimuth does but slowly varies in a certain area. In this work, a polynomial fitting method is used to reveal the noise gain trend along the range. Multiple experiments revealed that using a cubic polynomial fit provided better results and resulted in relatively fast computations. The coefficients of the cubic polynomial are determined via the method of least squares, as explicitly shown in Eq. 8:

$$\begin{aligned} \boldsymbol{S} &= \boldsymbol{R}\boldsymbol{A} \\ \boldsymbol{A} &= \left(\boldsymbol{R}^T\boldsymbol{R}\right)^{-1}\boldsymbol{R}^T\boldsymbol{S} \end{aligned} \tag{8}$$

where $\boldsymbol{S}$ represents the intensity value along the range, $\boldsymbol{R}$ is the polynomial variable matrix formed by the range index r, and $\boldsymbol{A}$ denotes the polynomial coefficient vector.

On the basis of the polynomial fitting results, the trend of the intensity variation along the range can be obtained. By normalizing with the median, the radial noise gain can be accurately determined. The range noise gain obtained from the fitting at azimuth x_0 can be written as:

$$\begin{cases} T_r(r,x_0) = a_0 + a_1 \cdot r + a_2 \cdot r^2 + a_3 \cdot r^3 \\ G_r(r,x_0) = \dfrac{T_r(r,x_0)}{\text{median}\left[T_r(r,x_0)\right]} \end{cases} \tag{9}$$

IV. Experiments

Experiments are conducted on GF-3 ScanSAR images to verify the effectiveness and robustness of the proposed method. Most descalloping methods [12]–[15] consider the impact of both stable and nonstable scenes on their effectiveness. Although the proposed method in this work does not require ScanSAR images to satisfy the assumption of a stable scene, experiments are conducted using both stable and nonstable scenes to validate its robustness. The Kalman filter and its improved method are currently the best-performing spatial domain descalloping methods. Therefore, the Kalman filter method is selected for comparative testing with the proposed method.

A. Relatively stable scene experiment

The Jarque-Bera (J-B) test is used to determine whether a scene is stable or nonstable [13]. Scenes with J-B values less than 2.5 are considered stationary and those with J-B values greater than 2.5 are considered nonstationary. The J-B test is calculated as follows:

$$\text{J-B} = \left[S^2/6 + (K-3)^2/24\right] \tag{10}$$

where S is the skewness and K is the kurtosis. S and K can be calculated as:

$$\begin{aligned} S &= \left[\frac{1}{n}\sum_{i=1}^{n}(x_i-\overline{x})^3\right] \Big/ \left[\frac{1}{n}\sum_{i=1}^{n}(x_i-\overline{x})^2\right]^{3/2} \\ K &= \left[\frac{1}{n}\sum_{i=1}^{n}(x_i-\overline{x})^4\right] \Big/ \left[\frac{1}{n}\sum_{i=1}^{n}(x_i-\overline{x})^2\right]^{2} \end{aligned} \tag{11}$$

where n is the number of observations and $\bar{x}$ is the mean. A portion of the data from one subswath in the GF-3 scan model is selected, and a calm sea area is used as the experimental area, as shown in Fig. 4(a). The area where J-B $= 0.3747$ serves as a typical representation of a stable scene. There is obvious scalloping present in the original ScanSAR image. Both the Kalman filter and the proposed method are used to eliminate scalloping from the original image. Fig. 4(b) and Fig. 4(c) show the descalloping results, and it is observed that the periodic noise is weakened. However, in Fig. 4(b), there are still obvious stripes in the left image, and better noise removal is achieved without obvious stripes in the right image. These findings are observed because the Kalman filter method assumes that scalloping does not change in the range, which is an unreasonable assumption that affects the descalloping effectiveness. As the proposed method considers the range spatial variant characteristic of scalloping, no obvious stripes are observed in Fig. 4(c), resulting in a better visual effect. Fig. 4(d) shows the quantitative evaluation of the denoising effect when the AGI is used. Fig. 4(d) shows that both the Kalman filter and the proposed method reduce periodic variations, indicating that these algorithms effectively eliminate scalloping. Moreover, the fluctuation of the yellow profile is smaller than that of the green profile, indicating that the proposed method is more effective.

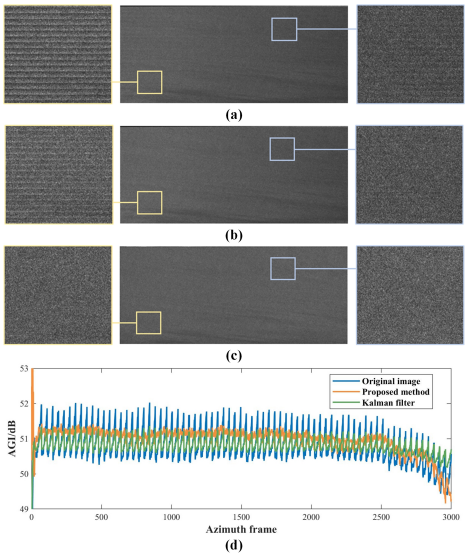

Fig. 4. Experimental results for relatively stable scenes. (a) original ScanSAR image, (b) Kalman filter, (c) proposed method, (d) AGI.

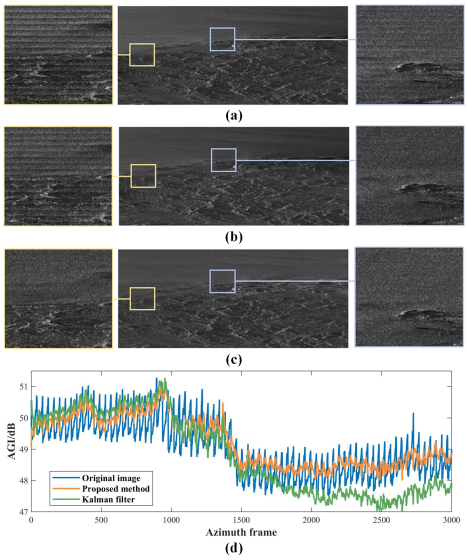

Fig. 5. Experimental results for nonstable scenes. (a) original ScanSAR image, (b) Kalman filter, (c) proposed method, (d) AGI.

B. Nonstable scene experiment

A nonstable scene is an image that contains a complex scene. Fig. 5(a) shows a sea-land interface area. The land area contains a rolling mountainous area, which is a nonstable scene with J-B $= 332.48$. In this scene, scalloping is more pronounced at the left and right edges of the image and weaker in the middle. Fig. 5(b) and Fig. 5(c) show the descalloping results obtained via the Kalman filter and the proposed method. The variation in scalloping in this range leads to the failure of the Kalman filter method. In Fig. 5(d), the yellow profile appears to deviate from the blue profile, indicating that the Kalman filter method not only fails to eliminate scalloping in this case but also changes the grayscale characteristics of the original image. In contrast, the proposed method achieves a better denoising effect in nonstable scenes

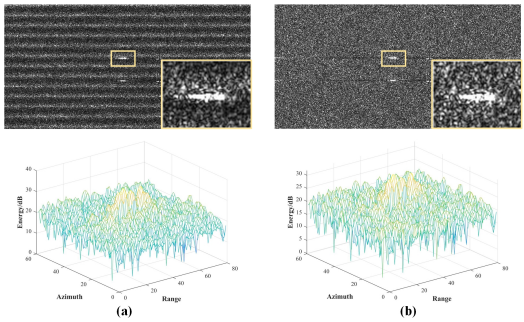

Fig. 6. Detail retention comparison experiment for Ship 1. (a) is the original image, and (b) is the proposed method result.

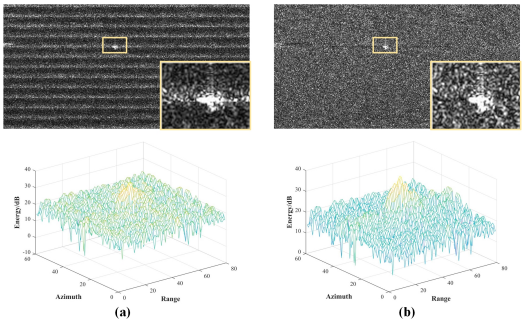

Fig. 7. Detail retention comparison experiment for Ship 2. (a) is the original image, and (b) is the proposed method result.

and exhibits strong robustness.

C. Detail retention comparison experiment

Another important criterion for evaluating the performance of descalloping methods is their ability to retain image details. In the following experiments, the performance of the proposed method in retaining image details is observed. Changes in the geometric and energetic properties of a ship's target before and after scalloping suppression are visually evaluated to assess the ability of the proposed method to retain target details. The results of the detailed retention comparison experiment are presented in Fig. 6 and Fig. 7.

Ship 1 in Fig. 6 is located in a region where scalloping is relatively weak. After the proposed method is applied, the geometric and contour features of the ship remain almost unchanged, and its energy remains essentially unchanged. Fig. 7 shows a scenario where Ship 2 is at a scalloping junction, which may lead to an inaccurate estimation of the noise intensity when the surrounding scallop noise is removed, affecting the descalloping effect. However, when the two sets of images in Fig. 7(a) and (b) are compared, it is found that the proposed method performs well in retaining the geometrical and energetic properties of Ship 2 and can effectively eliminate the scalloping around Ship 2. At the same time, there are noticeable black lines on both sides of the ship in Fig. 6 and Fig. 7. This is mainly due to the large brightness difference between the ship and the background in the original image, which causes a non-stationary phenomenon during fitting of the range noise gain. However, this does not affect the ship target itself. The above comparative analysis shows that the proposed method does not affect the image details and can better retain detail features.

V. Conclusion

The scalloping suppression problem in ScanSAR images has been studied in this work. In response to drawbacks such as poor robustness and high complexity in existing descalloping methods, a scalloping suppression method is proposed for ScanSAR images. The proposed method can eliminate scalloping in two steps, azimuthal correction error estimation and range noise gain fitting, has low complexity and is simple to implement. The performance of the proposed method is validated via GF-3 ScanSAR images collected from different scenes. The experimental results show that the proposed method can effectively suppress scalloping in ScanSAR images; at the same time, for ScanSAR images with scalloping in different scenes, the proposed method achieves excellent performance with good stability.

References

[1] X. Xiong, G. Jin, Q. Xu, X. Liu, and Q. Shi, "Robust multi-view UAV SAR image registration based on selective correlation of log gradient descriptor," *Int. J. Appl. Earth. Obs.*, vol. 127, pp. 103678, 2024.

[2] F. Argenti, A. Lapini, T. Bianchi, and L. Alparone, "A Tutorial on Speckle Reduction in Synthetic Aperture Radar Images," *IEEE Geosci. Remote Sens. Mag.*, vol. 1, no. 3, pp. 6–35, 2013.

[3] L. Zhong, X. Qiu, B. Han, and Y. Hu, "An Improved Descalloping Method Combined With Imaging Parameters for GaoFen-3 ScanSAR," *Remote Sens.*, vol. 12, no. 5, pp. 822, 2020.

[4] P. Martyn, J. Williams, J. Nicoll, R. Guritz, and T. Bicknell, "Calibration of the RADARSAT SWB processor at the Alaska SAR Facility," in *IGARSS '99*, Hamburg, Germany, 1999, pp. 2355–2359. DOI: 10.1109/IGARSS.1999.771508.

[5] A. P. Luscombe, "Taking A Broader View Radarsat Adds Scansar to Its Operations," in *IGARSS '88*, UK, 1988, pp. 1027–1032. DOI: 10.1109/IGARSS.1988.570512.

[6] R. Bamler, "Optimum Look Weighting for Burst-Mode and ScanSAR Processing," *IEEE Trans. Geosci. Remote Sens.*, vol. 33, no. 3, pp. 722–725, 1995.

[7] C. M. Vigneron, "RADIOMETRIC IMAGE QUALITY IMPROVEMENT OF SCANSAR DATA," Thesis of B. Eng. (High Distinction), Carleton Univ., Ottawa, ON, Canada, 1994.

[8] M. Shimada, "A New Method for Correcting ScanSAR Scalloping Using Forests and Inter-SCAN Banding Employing Dynamic Filtering," *IEEE Trans. Geosci. Remote Sens.*, vol. 47, no. 12, pp. 3933–3942, 2009.

[9] B. Han, C. B. Ding, L. H. Zhong, J. Y. Liu, Y. X. Hu, B. Lei. "The GF-3 SAR Data Processor," *Sensors*, vol. 18, no. 3, p. 835, 2018.

[10] D. Schiavulli, A. Sorrentino, and M. Migliaccio, "An Innovative Technique for Postprocessing Descalloping," *IEEE Geosci. Remote Sens. Lett.*, vol. 10, no. 3, pp. 424–427, 2013.

[11] R. Romeiser, J. Horstmann, M. J. Caruso, and H. C. Graber, "A Descalloping Postprocessor for ScanSAR Images of Ocean Scenes," *IEEE Trans. Geosci. Remote Sens.*, vol. 51, no. 6, pp. 3259–3272, 2013.

[12] M. Iqbal, J. Chen, W. Yang, P. Wang, and B. Sun, "Kalman Filter for Removal of Scalloping and Inter-Scan Banding in ScanSAR Images," *Prog. Electromagn. Res.*, vol. 132, pp. 443–461, 2012.

[13] W. Yang, Y. Li, W. Liu, J. Chen, C. Li, and Z. Men, "Scalloping Suppression for ScanSAR Images Based on Modified Kalman Filter With Preprocessing," *IEEE Trans. Geosci. Remote Sens.*, vol. 59, no. 9, pp. 7535–7546, 2021.

[14] W. Yang, J. D. Dong, X. W. An, H. C. Zeng, Z. Q. Ma, W. Liu, J. Chen, "An Adaptive Scalloping Suppression Method for ScanSAR Images Based on the Kalman Filter," *IEEE Trans. Geosci. Remote Sens.*, vol. 62, pp. 1–13, 2024.

[15] J. Tian, Y. Cai, W. Yu, and H. Fan, "An adaptive scalloping suppression method for spaceborne ScanSAR images based on pre-estimation and weighted filtering," *ISPRS J. Photogramm. Rem. Sens.*, vol. 190, pp. 267–278, Aug. 2022.